Anomalous conductivity tensor in the Dirac semimetal Na_3Bi

2016 EPL 114 27002

(http://iopscience.iop.org/0295-5075/114/2/27002)

A Letters Journal Exploring the Frontiers of Physics

April 2016

EPL, **114** (2016) 27002 www.epljournal.org
doi: 10.1209/0295-5075/114/27002

Anomalous conductivity tensor in the Dirac semimetal Na_3Bi

Jun Xiong[1], Satya Kushwaha[2], Jason Krizan[2], Tian Liang[1], R. J. Cava[2] and N. P. Ong[1]

[1] *Departments of Physics, Princeton University - Princeton, NJ 08544, USA*
[2] *Departments of Chemistry, Princeton University - Princeton, NJ 08544, USA*

received 31 January 2016; accepted in final form 28 April 2016
published online 11 May 2016

PACS 72.15.Gd – Electronic conduction in metals and alloys: Galvanomagnetic and other magnetotransport effects
PACS 72.20.My – Conductivity phenomena in semiconductors and insulators: Galvanomagnetic and other magnetotransport effects
PACS 75.47.De – Giant magnetoresistance

Abstract – Na_3Bi is a Dirac semimetal with protected nodes that may be sensitive to the breaking of time-reversal invariance in a magnetic field **B**. We report experiments which reveal that both the conductivity and resistivity tensors exhibit robust anomalies in B. The resistivity ρ_{xx} is B-linear up to 35 T, while the Hall angle exhibits an unusual profile approaching a step function. The conductivities σ_{xx} and σ_{xy} share identical power-law dependences at large B. We propose that these significant deviations from conventional transport result from an unusual sensitivity of the transport lifetime to B. The transport features are compared with those in Cd_3As_2.

In Dirac semimetals – the analogs of graphene in three-dimensional material – the bulk Dirac node is protected against gap formation via hybridization. The iridate pyrochlores were initially predicted [1] to have protected nodes, but crystal growth has been problematical. Recently, Young *et al.* [2] identified a class of materials in which time-reversal invariance (TRI) leads to node protection when the nodes occur at high-symmetry points (the time-reversal invariant momenta or TRIM). Subsequently, Wang *et al.* proposed that crystalline symmetry can protect Dirac nodes even when they occur away from TRIM. From band calculations, they identified Na_3Bi [3] and Cd_3As_2 [4] as Dirac semimetals. Photoemission [5–9] and scanning tunneling microscopy [10] recently confirmed that bulk Dirac nodes exist in both Na_3Bi and Cd_3As_2. Many groups [11–14] predict that, in Dirac and Weyl semimetals, charge pumping associated with the chiral anomaly can be observed in an intense magnetic field **B**. Recently, the chiral anomaly was detected in Na_3Bi as an enhanced conductivity "plume" that is locked to the direction of the applied magnetic field **B** [15]. The chiral anomaly experiments were performed on crystals in which the Fermi energy E_F is only 30 meV above the node. Here we report detailed transport experiments on Na_3Bi crystals in which E_F is $\sim$10$\times$ higher. We show that, even at low B, the breaking of TRI leads to robust anomalies in the conductivity tensor which appears to originate from a strongly B-dependent transport lifetime $\tau_{tr}(B)$. Among the anomalies are a robust B-linear magnetoresistence and an unusual step-like field profile of the Hall angle $\tan\theta$. The quantum oscillations also suggest that the Fermi surface (FS) has two frequency components. These unusual features show that even in crystals with large E_F the transport properties are highly unusual.

Na_3Bi single crystals were crystallized from the Na-rich compositions (90 and 95%) tuned to preclude the formation of the superconductor NaBi as an impurity phase [16,17] (growth details are published in ref. [18]). The crystal structure was confirmed by X-ray diffraction (the lattice structure is sketched in fig. 1(C)). The deep-purple crystals grow with the largest facets normal to the c-axis (001). To avoid deterioration of the crystals (which fully oxidize within 30 s of exposure to air), we attached contacts with Ag epoxy to the crystals inside an Ar glovebox and then covered them with oil before transferring to the cryostat (see ref. [15] for the detailed sample mounting process). The resistivity profile ρ *vs.* T is metallic (fig. 1(A)) with residual values ranging from 1.72 to 87 $\mu\Omega$cm. The Hall resistivity ρ_{yx} is n-type and strictly B-linear (fig. 1), with a nearly T-independent Hall coefficient $R_H = \rho_{yx}/B$ ($\hat{\mathbf{x}}||\mathbf{I}$ and $\hat{\mathbf{z}}||\hat{\mathbf{c}}$, where **I** is the current). Batch B and C samples were measured without post annealing, while G1 was post-annealed for 1 month. Table 1 lists the transport quantities measured in 8 samples. The samples B5, $\cdots$, B12, and C1 were measured without post annealing. Samples F1 and G1 were post-annealed

Table 1: Transport parameters in 8 samples of Na_3Bi. n_H is the Hall density inferred from R_H. k_F is the FS wave vector inferred from the period of the quantum oscillations and $n_F = g_v k_F^3/3\pi^2$ with $g_v = 2$. μ' is the transport mobility derived from $\rho(4\,\mathrm{K})$ and n_F, while μ is directly read from the profile of $\sigma_{xy}(B)$ in fig. 3(B) (main text). MR(9 T) is the MR ratio measured at 9 T. τ_{tr} is calculated from $\mu = ev_F\tau_{tr}/\hbar k_F$. f_1 and f_2 are the periods inferred from the SdH oscillations. The quantities ρ, n_H and μ are subject to the large uncertainty in estimating t ($\pm 50\,\mu$m), but k_F, n_F and μ_H are unaffected. F1 and G1 were post-annealed for 2 weeks and 1 month, respectively. The quantities $\rho(4\,\mathrm{K})$ and n_H are strongly affected by the large uncertainty in t, but k_F, n_F, μ and τ_{tr} are not.

Sample	$\rho(4\,\mathrm{K})$	$n_H\,(\mathrm{cm}^{-3})$	k_F	$n_F\,(\mathrm{cm}^{-3})$	μ'	μ	MR(9 T)	τ_{tr}	f_1	f_2
(units)	$\mu\Omega$cm	10^{19}	$\mathrm{Å}^{-1}$	10^{19}	cm^2/Vs	cm^2/Vs	–	ps	T	T
B5	34	–	0.083	3.8	–	–	5.69	–	–	–
B6	6.2	2.9	0.079	3.4	35000	39200	17	2.55	–	–
B10	7.5	6.5	0.081	3.6	13000	21600	9.62	1.49	–	–
B11	87	1.3	0.073	2.6	5500	–	10.5	–	–	–
B12	7.4	3.7	0.082	3.7	23000	27900	10.3	1.94	247.3	225.3
C1	5.1	8.9	0.084	4.0	13600	26500	16.2	1.93	223	202.8
F1	6.6	6.5	0.082	3.7	14600	30400	32.8	2.11	252.8	203.3
G1	1.72	4.6	0.085	4.1	78900	91000	97.1	6.71	241.8	225.3
E1	–	–	–	–	–	–	–	–	242.5	227.3

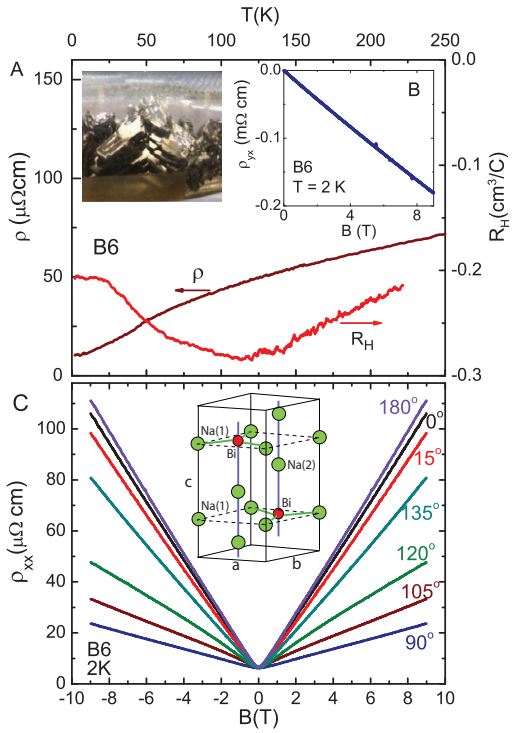

Fig. 1: (Color online) Magnetotransport in Na_3Bi. Panel A: the zero-field resistivity ρ and the Hall coefficient R_H *vs.* T (measured with $\mathbf{H}||\mathbf{c}$). The inset shows the crystals sealed in a vial. The largest facet is normal to $\hat{\mathbf{c}}$. Panel (B) shows the Hall resistivity ρ_{yx} *vs.* B measured at 2 K in B6. Panel (C): the H-linear magnetoresistance in sample B6 measured at 2 K at selected tilt angles θ to $\hat{\mathbf{c}}$. The MR ratio is largest at $\theta = 0°$ (and 180°). ($\mathbf{B} = \mu_0\mathbf{H}$ with μ_0 the vacuum permeability.) The crystal structure of Na_3Bi is sketched in the inset (adapted from ref. [5]).

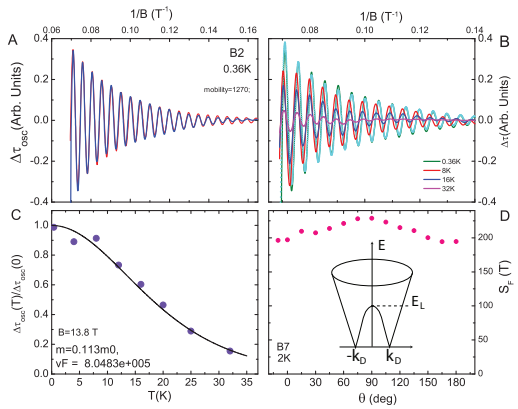

Fig. 2: (Color online) Torque measurements of the de Haas-van Alven (dHvA) oscillations in Na_3Bi. The dHvA oscillations (solid curve in panel (A)) can be fit well to the LK expression (dashed curve) with one period. From the damping *vs.* H (panel (A)) and the T-dependence (panels (B) and (C)), we obtain the Fermi surface section S_F, the effective mass $m^* = 0.11m_0$ (m_0 is the free mass), velocity $v_F = 8.05 \times 10^5$ m/s, and $\tau_Q = 8.16 \times 10^{-14}$ s. The plot of the peak fields B_{min} and B_{max} *vs.* the integers N (Panel D) yields S_F.

for 2 weeks and 1 month, respectively, before measuring. Because of difficulties related to prevention of oxidation, measurements of the crystal thickness t have a large uncertainty ($\pm 50\,\mu$m). This affects the estimates of ρ and n_H. However, the quantities inferred from Shubnikov-de Haas (SdH) oscillations (fig. 2) as we discuss below, as well as those from the field profile of $\sigma_{xy}(B)$ (fig. 3(B)), namely k_F, n_F, μ and τ_{tr} are unaffected by the uncertainties in t.

Figure 1(B) plots the MR curves in sample B6 for selected θ (the tilt angle between $\hat{\mathbf{c}}$ and the field $\mathbf{H} = \mathbf{B}/\mu_0$,

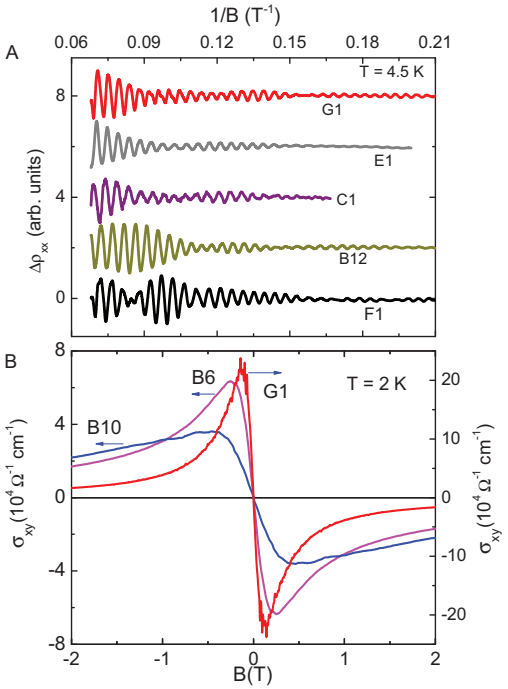

Fig. 3: (Color online) Panel A: curves of $\Delta\rho_{xx}$ showing modulation of the SdH amplitude. The beating pattern implies a small splitting of the fundamental SdH frequency. Panel B compares the Hall conductivity $\sigma_{xy}(B)$ in 3 samples at 2 K. In the 3 curves, the peak field $\pm B_\mu$ yields the values $\mu = 21640, 39250$ and $91000\,\mathrm{cm}^2/\mathrm{Vs}$ in B10, B6 and G1, respectively.

with μ_0 the vacuum permeability). As shown by the fan pattern, the MR ratio $\rho_{xx}(B)/\rho_{xx}(0)$ decreases rapidly as **H** is tilted into the a-b plane ($\theta \to 90°$).

All the samples display prominent Shubnikov-de Haas oscillations in $\rho_{xx}(B)$, from which the Fermi surface cross-section S_F and the Fermi wave vector k_F are determined. In addition, we have measured the de Haas-van Alven (dHvA) oscillations using torque magnetometry. Figure 2(A) shows the oscillatory component of the magnetization together with a fit to the Lifshitz-Kosevich (LK) expression. From fits to the dHvA amplitudes *vs.* $1/H$ and T (panels (B) and (C)), we determine the effective mass m^*, the Fermi velocity v_F and the quantum lifetime τ_Q. The carrier density $n = g_v k_F^3/3\pi^2$ (with the valley and spin degeneracies g_v and g_s both equal to 2) ranges from 2.6–$4.1 \times 10^{19}\,\mathrm{cm}^{-3}$, consistent with the Hall effect (table 1). In addition, by varying θ in the MR, we verify that the FS cross-section S_F is nearly spherical (fig. 2(D)).

Because of unintentional doping from vacancies, the Fermi energy E_F is high in the conduction band, as implied by the n-type sign of the Hall resistivity ρ_{yx}. The band calculations [3] predicted the existence of two Dirac nodes centered at $(0, 0, \pm k_D)$ caused by gap inversion (sketch in fig. 2(D)). As E_F rises in the conduction band, the two independent Dirac cones merge into a band with when E_F exceeds the Lifshitz-transition energy E_L. Recent ARPES experiments have confirmed the predicted dispersion and measured k_D to be $0.095\,\text{Å}^{-1}$ [5] and $0.10\,\text{Å}^{-1}$ [9] (see also [19]). However, because the ARPES spectra do not access states high above E_F, we cannot determine at present the actual sign of $E_F - E_L$ in the conduction band.

We further uncover an interesting and persistent feature in the SdH oscillations, *i.e.* a weak beating pattern in the SdH oscillations. Figure 3(A) shows the SdH traces from 5 samples. The Fourier spectra of the oscillations reveal two frequencies f_1 and f_2 corresponding to two values of S_F differing by $\sim 16\%$ (values reported in table 1). The beating suggests that the orbits may reflect quantum interference between the two orbits. A systematic trend in the splitting $f_1 - f_2$ has not been found, but we hope to explore them further in high-mobility crystals.

The mobility μ of each sample is directly measured from the field profile of the Hall conductivity σ_{xy}. As shown in fig. 3(B), $\sigma_{xy}(B)$ has the characteristic dispersion-resonance profile produced by cyclotron motion of the carriers. By the Bloch-Boltzmann theory, the extrema in $\sigma_{xy}(B)$ occur at the peak fields $\pm B_\mu$, with $1/B_\mu = \mu$. With increasing μ, from sample B10 ($\mu = 21640\,\mathrm{cm}^2/\mathrm{Vs}$) to B6 ($39250\,\mathrm{cm}^2/\mathrm{Vs}$) and G1 ($91000\,\mathrm{cm}^2/\mathrm{Vs}$), the peak field B_μ systematically decreases. The variation in μ strongly influences the Hall-angle profile (see below). Using $\mu = ev_F\tau_{tr}/\hbar k_F$, we find that the transport lifetime τ_{tr} exceeds τ_Q by a ratio R_τ = 10-20 (R_τ is expected to exceed 1 since τ_Q reflects broadening due to all scattering processes). In Cd_3As_2, R_τ is as large as 10^4 [20].

In the relaxation-time *ansatz*, the Boltzmann equation describing changes to the distribution function $f_{\mathbf{k}}$ caused by an electric field **E** is expressed as [21]

$$e\mathbf{E}\cdot\mathbf{v}\frac{\partial f^0_{\mathbf{k}}}{\partial E_{\mathbf{k}}} + e\mathbf{v}\times\mathbf{B}\cdot\frac{\partial g_{\mathbf{k}}}{\partial \mathbf{k}} = -\frac{g_{\mathbf{k}}}{\tau_{tr}}, \qquad (1)$$

where e is the elemental charge and $g_{\mathbf{k}} = f_{\mathbf{k}} - f^0_{\mathbf{k}}$, with $f^0_{\mathbf{k}}$ the Fermi-Dirac function. $E_{\mathbf{k}}$ and velocity **v** are, respectively, the energy and velocity at state **k**. The *ansatz* yields the conductivity tensor σ_{ij}, with

$$\sigma_{xx} = ne\mu/D, \qquad \sigma_{xy} = ne\mu^2 B/D, \qquad (2)$$

where $D = 1 + (\mu B)^2$. From eq. (2), the ratio $\sigma_{xy}/\sigma_{xx} = \mu B$, which is the Hall angle $\tan\theta$, is linear in B. By contrast, the resistivity ρ_{xx} is B-independent because the Hall electric field E_y exactly balances the Lorentz force. Significantly, $\sigma_{xx} \sim 1/B^2$ decreases much faster than $\sigma_{xy} \sim 1/B$ when $\mu B \gg 1$. These standard predictions assume that τ_{tr} (hence μ) is a constant independent of B. In conventional metals and semimetals in the impurity-scattering regime (elastic scattering), this assumption is firmly established; the predicted trends are a cornerstone of semiclassical transport.

In Na_3Bi, however, the observed field dependences of the diagonal elements σ_{xx} and ρ_{xx} disagree in an essential way from the standard predictions (only $\rho_{yx}(B)$ appears conventional). As we noted in fig. 1, the resistivity

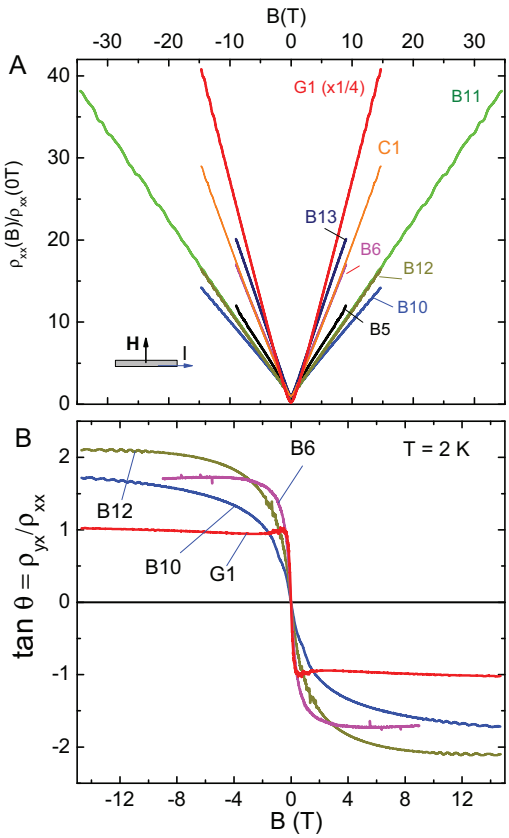

Fig. 4: (Color online) Robust H-linear magnetoresistance in Na_3Bi (panel (A)). In the 8 samples shown, $\rho_{xx}(B)$ is measured with $\mathbf{H}||\hat{\mathbf{c}}$ at 2 K in all cases except in B11 (at 1.6 K). In B11, the MR persists without observable deviation to 35 T. A general trend is that the MR increases with μ, from ~ 14 (at 15 T) in B10, to ~ 160 in G1 (which has the highest μ) (the MR in G1 is plotted in $\frac{1}{4}$ scale). In panel (B), the field profile of $\tan\theta = \rho_{yx}/\rho_{xx}$ is compared in 4 samples. As H increases, $\tan\theta$ rapidly saturates to an H-independent value, which implies the anomalous relationship $\tau_{tr} \sim 1/H$. In G1, the change occurs at 0.5 T.

increases linearly with B instead of saturating. A B-linear MR is rare in conventional conductors (see Abrikosov's comments [22]; we exclude metals with open orbits [21]). In addition to the present report and ref. [15], the unusual B-linear transverse MR has been observed in (type-B crystals) of the Dirac semimetal Cd_3As_2 [20], as well as in the topological insulator Bi_2Te_3 [23]. These results have stimulated renewed theoretical interest in linear MR. In ref. [24], it is predicted that diffusion of the guiding centers in weak disorder potentials varying on lengthscales much longer than the cyclotron radius leads to linear transverse MR even up to 300 K.

To persuade ourselves that the B-linear MR is pervasive in Na_3Bi, we have investigated 8 samples (table 1). Figure 4(A) shows that the B-linear MR is a very robust feature in Na_3Bi. Across the samples, the MR ratio (measured at 15 T) increases from ~ 14 in B10, to 163 in G1 (the sample with the highest μ). In B11, we show that

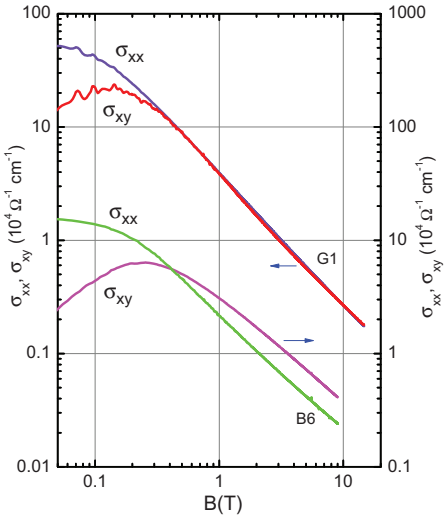

Fig. 5: (Color online) Log-log plots of σ_{xx} and σ_{xy} *vs.* B in G1 and B6. Consistent with eq. (3), both quantities approach the same power law $B^{-\beta}$ when B exceeds 0.3 and 2 T in G1 and B6, respectively. The measured β is 1.15 and 1.0 in G1 and B6, respectively. Curves for B6 are shifted vertically.

the B-linear profile extends to 35 T with no evidence of deviation.

A second dramatic anomaly is seen in the Hall-angle profile. In fig. 4(B), we compare $\tan\theta$ measured in four samples with increasing μ, B10, B12, B6 and G1. As shown, $\tan\theta$ initially rises very rapidly in weak B at a rate dictated by the mobility, but saturates to a plateau value at large B. Whereas the saturation is gradual in the samples with low mobility (B10 and B12), the rise becomes abrupt in higher-mobility samples (B6 and G1). In G1, especially, the profile resembles a step-function profile. $\tan\theta$ assumes a virtually B-independent value from $B = 0.5$ to 15 T instead of increasing linearly with B. Since $\tan\theta = \mu B$, the simplest interpretation of the step-function profile is that, starting in weak B, the transport lifetime varies with B as

$$\tau_{tr} \sim 1/B. \tag{3}$$

The merit of eq. (3) is that it also accounts for the B-linear MR profile, *i.e.* $\rho_{xx} = 1/ne\tau_{tr} \sim B$. Interestingly, with eq. (3), the high-field B-dependence of σ_{xx} is reduced by one power of B to $\sigma_{xx}(B) \sim 1/B$ (eq. (2)), but leaves that of $\sigma_{xy} \sim 1/B$ unchanged because μ cancels out at large B. Hence both σ_{xx} and σ_{xy} vary as $1/B$ at large B, consistent with the step profile of $\tan\theta$.

To verify this, we plot the B-dependences of σ_{xx} and σ_{xy} in log-log scale for the two high-mobility samples B6 and G1 (fig. 5). In both samples, the two conductivities have the same power-law dependence $B^{-\beta}$ above a relatively low B. Consistent with the behavior of $\tan\theta$, this occurs at $B = 2$ T and 0.3 T in B6 and G1, respectively. The measured value of β is 1.0 in B6, but is slightly larger (1.15) in G1.

We also notice the strong similarities (and some differences) between the magnetoresistance (MR) results in Na_3Bi and those in Cd_3As_2. In ref. [20], the Cd_3As_2 samples investigated fall into two groups. Set-A samples are needle-shaped single crystals, while Set-B samples are polycrystals cut from the boule. A B-linear MR very similar to the MR observed in Na_3Bi is observed in all Set-B samples as well as in the Set-A crystals with "lower mobility" (100000 to 150000 cm^2/Vs). In Set-A crystals displaying ultrahigh mobility (150000 to 10^7 cm^2/Vs), the MR evolves to a B^2 profile.

The ratio of the transport to quantum lifetimes, $R_\tau = \tau_{tr}/\tau_Q$, reaches very large values (10^4) in the ultrahigh mobility Cd_3As_2 crystals. Liang *et al.* [20] infer that the ultrahigh mobilities likely arise from a protection mechanism that strongly suppresses back-scattering for currents flowing along the needle axis when time-reversal invariance (TRI) prevails. Application of a magnetic field B breaks TRI and results in the lifting of the protection, hence a giant MR. The MR ratios attain values significantly larger than those seen in Na_3Bi.

It seems to us that a crucial difference between the two Dirac semimetals is that the scattering rate $1/\tau_{tr}$ in Cd_3As_2 is highly anisotropic especially in crystals with the highest mobilities (as determined using the Montgomery technique). The anisotropy notwithstanding, the main finding is the strong effect of B on $1/\tau_{tr}$, similar to eq. (3). Because its scattering rate $1/\tau_{tr}$ is nearly isotropic, Na_3Bi provides a simpler platform to unravel the mechanism underlying deviations from conventional transport.

Theoretically, in the Weyl semimetal, the Weyl nodes which come in pairs act as sources and sinks of Berry curvature (Chern flux) [1,11–14]. To realize a finite Berry curvature $\vec{\Omega}(\mathbf{k})$, TRI must be broken in the Weyl semimetal. The 3D Dirac semimetal may be regarded as the limiting case when TRI is restored. In this limit, the Weyl nodes coincide in $\mathbf{k}$ space but are prevented from hybridizing by crystalline symmetry. Conversely [3], one expects that, in a Dirac semimetal, the breaking of TRI by an applied $\mathbf{B}$ will render $\vec{\Omega}(\mathbf{k})$ finite, and lead to essential changes in its FS best detected by transport experiments.

The large negative longitudinal MR associated with the chiral anomaly is most pronounced in Na_3Bi crystals with E_F close to the node [15]. However, as shown by the present results, even in crystals with large E_F, the finite Berry curvature seems to lead to major anomalous features in the conductivity tensor elements σ_{ij}. The results in both Na_3Bi and Cd_3As_2 [20] invite a re-examination of transport in Dirac semimetals.

* * *

We thank Andrei Bernevig and Ashvin Vishwanath for valuable discussions. NPO is supported by the Army Research Office (ARO W911NF-11-1-0379). RJC and NPO are supported by a MURI grant on Topological Insulators (ARO W911NF-12-1-0461). The crystal growth effort was supported by the US National Science Foundation (grant No. DMR 1420541). TL acknowledges scholarship support from the Japan Student Services Organization. Some of the experiments were performed at the National High Magnetic Field Laboratory, which is supported by National Science Foundation Cooperative Agreement No. DMR-1157490, the State of Florida, and the U.S. Department of Energy.

REFERENCES

[1] Wan X., Turner A. M., Vishwanath A. and Savrasov S. Y., *Phys. Rev. B*, **83** (2011) 205101.
[2] Young S. M., Zaheer S., Teo J. C. Y., Kane C. L., Mele E. J. and Rappe A. M., *Phys. Rev. Lett.*, **108** (2012) 140405.
[3] Wang Z., Sun Y., Chen X. Q., Franchini C., Xu G., Weng H., Dai X. and Fang Z., *Phys. Rev. B*, **85** (2012) 195320.
[4] Wang Z., Weng H., Wu Q., Dai X. and Fang Z., *Phys. Rev. B*, **88** (2013) 125427.
[5] Liu Z. K., Zhou B., Zhang Y., Wang Z. J., Weng H. M., Prabhakaran D., Mo S.-K., Shen Z. X., Fang Z., Dai X., Hussain Z. and Chen Y. L., *Science*, **343** (2014) 864.
[6] Neupane M., Xu S.-Y., Sankar R., Alidoust N., Bian G., Liu C., Belopolski I., Chang T.-R., Jeng H.-T., Lin H., Bansil A., Chou F. and Hasan M. Z., *Nat. Commun.*, **5** (2014) 3786.
[7] Liu Z., Jiang J., Zhou B., Wang Z., Zhang Y., Weng H., Prabhakaran D., Mo S., Peng H., Dudin P. *et al.*, *Nat. Mater.*, **13** (2014) 677.
[8] Borisenko S., Gibson Q., Evtushinsky D., Zabolotnyy V., Büchner B. and Cava R. J., *Phys. Rev. Lett.*, **113** (2014) 027603.
[9] Xu S.-Y., Liu C., Kushwaha S., Chang T.-R., Krizan J., Sankar R., Polley C., Adell J., Balasubramanian T., Miyamoto K. *et al.*, arXiv:1312.7624v1 (2013).
[10] Jeon S., Zhou B. B., Gyenis A., Feldman B. E., Kimchi I., Potter A. C., Gibson Q. D., Cava R. J., Vishwanath A. and Yazdani A., *Nat. Mater.*, **13** (2014) 851.
[11] Son D. T. and Spivak B. Z., *Phys. Rev. B*, **88** (2013) 104412.
[12] Burkov A. A., Hook M. D. and Balents L., *Phys. Rev. B*, **84** (2011) 235126.
[13] Hosur P. and Qi X., *C. R. Phys.*, **14** (2013) 857.
[14] Parameswaran S. A., Grover T., Abanin D. A., Pesin D. A. and Vishwanath A., *Phys. Rev. X*, **4** (2014) 031035.
[15] Xiong J., Kushwaha S. K., Liang T., Krizan J. W., Hirschberger M., Wang W., Cava R. J. and Ong N. P., *Science*, **350** (2015) 413.
[16] Kushwaha S. K., Krizan J. W., Xiong J., Klimczuk T., Gibson Q. D., Liang T., Ong N. P. and Cava R. J., *J. Phys.: Condens. Matter*, **26** (2014) 212201.
[17] Brauer G. and Zintl E., *Z. Phys. Chem. B*, **37** (1937) 323.
[18] Kushwaha S. K., Krizan J. W., Feldman B. E., Gyenis A., Randeria M. T., Xiong J., Xu S.-Y.,

Alidoust N., Belopolski I., Liang T. *et al.*, *APL Mater.*, **3** (2015) 041504.
[19] Zhang Y., Zhou B., Kim Y., Hussain Z., Shen Z.-X., Chen Y. and Mo S.-K., *Appl. Phys. Lett.*, **105** (2014) 031901.
[20] Liang T., Gibson Q., Ali M. N., Liu M., Cava R. and Ong N., *Nat. Mater.*, **14** (2015) 280.
[21] Ziman J. M., *Electrons and Phonons* (Oxford University Press) 1960.
[22] Abrikosov A. A., *Phys. Rev. B*, **58** (1998) 2788.
[23] Qu D.-X., Hor Y. S., Xiong J., Cava R. J. and Ong N. P., *Science*, **329** (2010) 821.
[24] Song J. C. W., Refael G. and Lee P. A., *Phys. Rev. B*, **92** (2015) 180204.